

## Mimicking bone remodeling to optimize hierarchical, multi-material 3D printed metamaterials

Saldívar, M. C.; Tay, E.; Pahlavani, H.; Doubrovski, E. L.; Mirzaali, M. J.; Zadpoor, A. A.

**DOI**

[10.1016/j.apmt.2025.102722](https://doi.org/10.1016/j.apmt.2025.102722)

**Publication date**

2025

**Document Version**

Final published version

**Published in**

Applied Materials Today

**Citation (APA)**

Saldívar, M. C., Tay, E., Pahlavani, H., Doubrovski, E. L., Mirzaali, M. J., & Zadpoor, A. A. (2025). Mimicking bone remodeling to optimize hierarchical, multi-material 3D printed metamaterials. *Applied Materials Today*, 44, Article 102722. <https://doi.org/10.1016/j.apmt.2025.102722>

**Important note**

To cite this publication, please use the final published version (if applicable). Please check the document version above.

**Copyright**

Other than for strictly personal use, it is not permitted to download, forward or distribute the text or part of it, without the consent of the author(s) and/or copyright holder(s), unless the work is under an open content license such as Creative Commons.

**Takedown policy**

Please contact us and provide details if you believe this document breaches copyrights. We will remove access to the work immediately and investigate your claim.



# Mimicking bone remodeling to optimize hierarchical, multi-material 3D printed metamaterials

M.C. Saldívar<sup>a,#</sup>, E. Tay<sup>a,#</sup> , H. Pahlavani<sup>a</sup> , E.L. Doubrovski<sup>b</sup>, M.J. Mirzaali<sup>a,\*</sup> ,  
A.A. Zadpoor<sup>a</sup>

<sup>a</sup> Department of Biomechanical Engineering, Faculty of Mechanical, Maritime, and Materials Engineering, Delft University of Technology (TU Delft), Mekelweg 2, Delft 2628 CD, The Netherlands

<sup>b</sup> Faculty of Industrial Design Engineering (IDE), Delft University of Technology (TU Delft), Landbergstraat, 15, Delft CE 2628, The Netherlands

## ARTICLE INFO

### Keywords:

Multi-material 3D printing  
Voxel-based 3D printing  
Hierarchy  
Remodeling optimization  
Soft-hard interface design  
Metamaterials

## ABSTRACT

In this study, by mimicking bone tissue adaptation, we introduce a hierarchical design approach to optimize the mechanical performance of auxetic metamaterials. Using a multi-material voxel-based 3D printer, we rationally position soft and hard phases at the voxel level based on a bone-inspired remodeling algorithm that maintains the homeostasis of strain energy density. This process introduces an additional length scale within the structure, leading to (1) a significant expansion of the envelope of achievable elastic properties, (2) more homogeneous strain energy distributions, and (3) up to 78 % stronger metamaterials compared to initial designs. Our results demonstrate that this bone-mimicking design approach enables the emergence of an intermediate length scale between the unit cell and voxel scales, which is responsible for the observed improvements in mechanical performance. Taken together, these findings highlight the potential of biomimetic remodeling for the rational design of stress-worthy, multiscale mechanical metamaterials that combine unusual elastic properties with high mechanical performance.

## 1. Introduction

In recent years, there has been a paradigm shift in the materials design community towards creating structures with unusual properties (e.g., negative Poisson's ratio (=auxetic), ultra-stiffness or flexibility, and shape morphing) [1–5]. Auxetic unit cells are extensively studied in the design of metamaterials and meta-structures for several reasons. First, there is a growing body of research demonstrating that unit cells with auxetic properties can positively influence bone cell responses, particularly when these properties are decoupled from the other mechanical and morphological properties of the scaffolds [6–9]. Second, these unit cells have shown superior compressive fatigue performance as compared to non-auxetic unit cells [10–12]. Finally, auxetic meta-biomaterials can be used in the design of hybrid meta-implants, where they contribute to better bone-implant interfaces [13–15]. In areas subjected to tensile loading, auxetic materials can improve bone-implant connection, reducing the risk of bone loosening. This could potentially lead to the prevention of implant-associated infections.

Therefore, controlling the Poisson's ratio can be considered as a crucial design tool for developing meta-biomaterials and meta-implants with tailored properties. These aforementioned properties, such as elastic stiffness and Poisson's ratio, can even go beyond their mutually exclusive theoretical limits [10,14,16–18]. Although various methods have been proposed to decouple these properties (e.g., introducing degrees of non-affinity and multi-material metamaterials) [19,20], such meta-material design techniques have several limitations. For example, the junctions of the structural elements constituting the microarchitectures of many such designs effectively function as hinges, thereby causing non-homogenous strain distributions and considerable degrees of stress concentration [21–23]. These strain concentrations promote early crack initiation and growth, leading to diminished mechanical performance and premature failure. Addressing such design issues while also maintaining and preferably expanding the envelope of possible elastic properties is an open challenge.

Living organisms have been facing similar challenges in their load-bearing tissues where combining lightweight, high mechanical

\* Corresponding author.

E-mail address: [m.j.mirzaali@tudelft.nl](mailto:m.j.mirzaali@tudelft.nl) (M.J. Mirzaali).

# Both authors contributed equally to this study.

performance, and exotic properties (e.g., negative or zero values of the Poisson's ratio [24,25]) has been instrumental in maximizing their 'fitness' for survival. Through millions of years of evolution, living organisms have developed ingenious strategies to satisfy these seemingly incompatible design requirements. Two of these strategies include the hierarchical arrangement of microarchitectural features and combining soft (e.g., collagen) and hard (e.g., hydroxyapatite) phases [26–29]. This seamless integration of hierarchy and multiple phases within the fabric of load-bearing tissues is rooted in the evolutionary processes that can circumvent the infamous material property trade-off (e.g., the incompatibility between high strength and high toughness in engineering materials) [30,31]. An important example of such living materials is bone, which, through a remodeling process, optimizes its mechanical response to the mechanical loads it experiences [32,33]. The remodeling process occurs at different length scales, from the level of the bone tissue to the cellular level, and is influenced by various factors, including biochemical and biomechanical cues. In this study, we focus only on the mechanical cues for the bone remodeling process and employ theories based on the strain energy density to predict these remodeling processes [34–40].

Here, we mimic the remodeling process of living bone to address the open challenge regarding the design of stress-worthy mechanical metamaterials with unusual elastic properties. While bone tissue adaptation has been linked to the optimal mechanical performance in trabecular bone [41,42], direct applications of this approach to the design of mechanical metamaterials are yet to be reported [43]. Our biomimetic design approach involves the introduction of a microarchitecture hierarchy with multiple length scales and the rational positioning of a soft and a hard phase at the individual voxel level using a multi-material voxel-based additive manufacturing technique [44–47]. We used a modified theoretical model of the bone tissue process working on the basis of homeostatic strain energy density to optimize the distribution of the hard and soft voxels within the fabric of each re-entrant or honeycomb unit cell of an auxetic and a conventional metamaterial, thereby introducing two hierarchical length scales (i.e., unit cell and voxel). This approach differs from similar works, which have utilized Bayesian optimization, deep learning, and evolutionary algorithm approaches [48–51]. In particular, our approach focuses on the morphogenesis of hierarchical multi-material structures in response to mechanical stimuli, as opposed to the aforementioned data-oriented and statistical optimization approaches. We then evaluated the elastic properties and stress worthiness of the developed metamaterials using both computational models and experiments. The elastic properties and mechanical performance of the designed mechanical metamaterials were then benchmarked against control groups consisting of single-scale, monolithic specimens.

This work advances prior research by moving beyond the direct voxel-based digitization of hard and soft phases to an adaptive design methodology inspired by bone remodeling. Unlike previous approaches that relied on predetermined voxel arrangements, the current study introduces a hierarchical remodeling algorithm that optimizes metamaterials' internal architecture based on mechanical loading conditions.

## 2. Materials and methods

### 2.1. Initial unit cell design

We designed two generic unit cells for our analysis, a re-entrant (auxetic) and regular (non-auxetic) honeycomb with entrant angles  $\theta$  of  $-20^\circ$  and  $20^\circ$ , respectively (Fig. 1A). These unit cells were chosen due to their relative ease of parameterization, allowing for an analogous comparison between regular and auxetic deformations, and their prevalence in similar studies exploring multi-material metamaterials [52–54]. We also considered other unit cell types (i.e., tetra-anti-chiral and a 2D equivalent of a hexaround cell, see Section 3.3) to verify the results obtained using the initial unit cells. We utilized an in-house

MATLAB script (R2018b, MathWorks, USA) to generate one-quarter representations of these designs in a voxel form, with dimensions of 80, 40, and 4 voxels in height ( $H_{uc}$ ), width ( $W_{uc}$ ), and out-of-plane thickness ( $L_{uc}$ ), respectively. The thickness of each strut consisted of 12 voxels, equivalent to 30 % of  $W_{uc}$ , and the dimension of each voxel was  $42 \times 84 \times 27 \mu\text{m}^3$ . For both angles, we used a 3D Stucki dithering technique [55] to obtain several unit cells with varying ratios of the volume of the hard phase to that of the total volume ( $\rho = 17\%$ ,  $33\%$ ,  $50\%$ ,  $67\%$ , or  $83\%$ ) (Figure S1 of the supplementary document). We completed the unit cells by mirroring the quarter designs.

### 2.2. Numerical simulations

An in-house Python (v2.7.3) script allowed the integration of the designs into a commercial nonlinear FEM package (Abaqus Standard v.6.14, Dassault Systèmes Simulia, France) to generate quasi-static finite element method (FEM) models (Fig. 1B). This script converted the voxel designs into hexahedral element (C3D8) meshes and assigned the material properties of each voxel. After performing a mesh convergence study (section S1 of the supplementary document), we selected a 1:1 ratio of elements to voxel for simulating the bone tissue adaptation process. To validate the experimental results, we prepared additional simulations with a 64:1 ratio (i.e., 64 elements per voxel). We modeled the hard phase using a linear elastic constitutive equation (i.e., elastic modulus  $E = 2651$  MPa, Poisson's ratio  $\nu = 0.4$ ) while a hyperelastic constitutive model was used for the soft one (i.e., Ogden,  $N = 1$ , shear modulus  $\mu_1 = 0.266$  MPa, constants  $\alpha_1 = 3.006$  and  $D_1 = 0.113$ ) [56]. After assigning periodic boundary conditions to the unit cells, we simulated two displacement-controlled uniaxial tensile tests per design (i.e., along directions 1 and 2) with an equivalent strain of  $\epsilon = 0.25\%$  each. From these simulations, we extracted the reaction forces ( $f_1$  and  $f_2$ ) and displacements ( $u_{11}$ ,  $u_{12}$ ,  $u_{22}$ , and  $u_{21}$ ) of each unit cell from which we calculated the respective elastic properties (i.e.,  $E_{11} = (f_1/L_{uc}u_{11})$ ,  $E_{22} = f_2/(L_{uc}u_{22})$ ,  $\nu_{12} = -u_{12}/u_{11}$ , and  $\nu_{21} = -u_{21}/u_{22}$ ). Finally, we extracted the vectors containing the strain energy density (SED) of each voxel of the entire lattice (i.e.,  $U_1$  and  $U_2$ ).

### 2.3. Bone-mimicking computational model for rational distribution of soft and hard voxels

We defined our bone-mimicking optimization routine as an iterative procedure where the voxels within the unit cells were continuously committed or converted to a specific material based on their relative strain energy density (SED) (Fig. 1C). This is based on the underlying principle of bone remodeling in response to SED as a stimulus [41]. For every iteration, after running the simulations with loading in both directions, the algorithm extracted the SED of each voxel ( $SED_1$  and  $SED_2$ , for directions 1 and 2, respectively). Then, to remove the anisotropic effects of the unit cell, it performed min-max feature scaling on these vectors ( $U = (SED - \min(SED))/(\max(SED) - \min(SED))$  for directions 1 and 2), from which it calculated the effective SED vector  $S$  as:

$$S = \lambda U_1 + (1 - \lambda) U_2 \quad (1)$$

where  $\lambda$  is a weighting parameter. Four operations are then concurrently performed using this ranked vector. First, the soft voxels with the highest effective SED (i.e., 0.5 % of all the voxels within the unit cell) were converted into hard voxels. Conversely, the same number of hard voxels with the lowest effective SED values were converted to soft voxels to maintain a consistent  $\rho$  during the whole process. After converting to any material, the voxels were committed to remain as such to prevent them from continuously oscillating between hard and soft voxels. For the third operation, the soft elements with the lowest effective SED (i.e., 0.5 % of all the voxels) were assumed to show a sufficient capacity for energy absorption and were committed to the soft phase for the future iterations. In the last operation, the same number of hard voxels with the

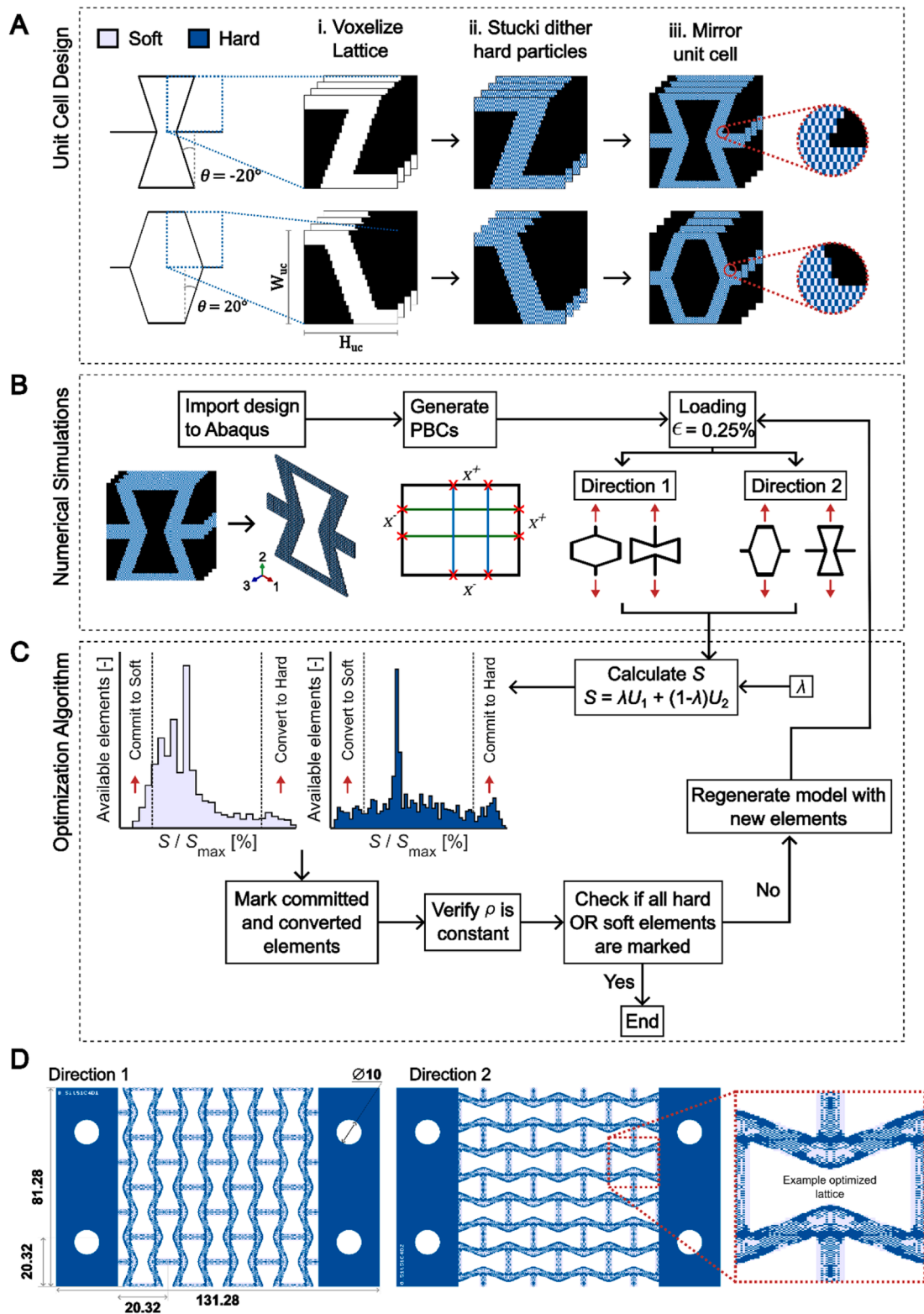


**Fig. 1.** Schematic drawings illustrating the entire design and optimization process. A) The process used for the generation of the initial unit cell designs where a quarter of the unit cell geometries are converted into 4 stacks of  $40 \times 80$  voxels (i.) and hard and soft voxels are distributed within the struts (ii.) prior to mirroring them into a complete unit cell (iii.). B) The generated designs are then imported into a FEM software suite where periodic boundary conditions (PBCs) are assigned, and two quasi-static tensile tests are simulated along both orthogonal directions. C) The SED of each voxel is then used to commit or convert the voxels to a material type (i.e., hard or soft) while maintaining a constant number of hard voxels. The process of simulation and remodeling continues until all the voxels have been committed to a specific material type. D) The representative design of the additively manufactured  $4 \times 4$  unit cell lattices for experimental validation (off-plane thickness = 3 mm).

highest effective SED values were committed to the hard phase. This process is repeated in each iteration until all the voxels have committed to either the hard or the soft phase. Since the values within the ranked vector  $\mathbf{S}$  drive the remodeling of the unit cell, the parameter  $\lambda$  determines the anisotropic bias of the remodeling process, where  $\lambda = 0$  and  $\lambda = 1$  fully bias the remodeling process towards direction 1 or direction 2, respectively, while  $\lambda = 0.5$  does not prioritize either one of the directions. We performed a detailed analysis of the SED redistribution achieved by the algorithm for a single representative design (*i.e.*,  $\theta = -20^\circ$ ,  $\rho = 50\%$ ). Towards this end, we calculated the normalized SED vectors of the unit cells (*i.e.*, the SED value of each voxel divided by the total SED within the unit cell) throughout the remodeling process for all the evaluated  $\lambda$  values.

While our approach is inspired by biological bone remodeling, it is not intended as a strict mathematical optimization method with a pre-defined objective function. Instead, the algorithm follows an adaptive redistribution process based on local SED values, similar to how bone tissue responds to mechanical loading. This bio-inspired strategy prioritizes minimizing local SED concentrations rather than seeking a globally optimal material configuration. Unlike topology optimization, which typically relies on iterative cost function minimization, our method ensures gradual and physically meaningful material redistribution without abrupt or non-physical transitions.

#### 2.4. Voxel-by-voxel multi-material 3D printing

A PolyJet multi-material 3D printer (ObjetJ735 Connex3, Stratasys® Ltd., USA) with voxel-level control enabled (voxel resolution of 300×600 dpi with layers of 27 μm) was used to manufacture the validation specimens. For the hard and soft phases, we used the VeroCyan™ (RGD841, Stratasys® Ltd., USA) and Agilus30™ Clear (FLX935, Stratasys® Ltd., USA) UV-curable photopolymers, respectively. We defined two lattice configurations for testing along either direction 1 or 2 (Fig. 1D) and based their dimensions on the existing literature [45,57]. After a comparative study of multiple lattice sizes (Section S2 of the supplementary document), we determined that 4 × 4 unit cells per specimen with a voxel size of 8 μm<sup>3</sup> minimized unwanted PolyJet material mixing while still reflecting the periodicity of the designed lattices. We selected eight different designs for manufacturing (Table 1), from which we generated the required stacks of binary images as input for the 3D printer, with each bit specifying whether or not each phase is deposited at the position of the corresponding voxel. Three specimens were printed from each design.

#### 2.5. Mechanical testing and full-field strain measurements

We performed quasi-static tensile tests on the 3D printed specimens to validate our computational analyses and evaluate the performance of the optimized designs. We used a mechanical test bench (Instron ElectroPuls™ E10000, load cell = 10 kN) to apply a deformation of 2 mm/min until failure. We registered the time ( $t$ ) and force ( $f$ ) signals at a frequency of 100 Hz. Prior to testing, the specimens were coated with a white paint followed by a black speckle pattern. We then measured the

**Table 1**

The designs selected for fabrication and mechanical testing. \*These designs were used for control and were made of only hard material.

Name	$\theta$ [°]	$\rho$ [%]	$\lambda$	Iteration	Direction
Hard <sub>1</sub> *	-20	100	-	-	1
Hard <sub>2</sub> *	-20	100	-	-	2
$E_{1,initial}$	-20	50	-	0	1
$E_{2,initial}$	-20	50	-	0	2
$E_{1,max, \lambda_{0.75}}$	-20	50	0.75	22	1
$E_{1,max, \lambda_{0.50}}$	-20	50	0.50	50	1
$E_{2,max, \lambda_{0.50}}$	-20	50	0.50	50	2
$E_{2,max, \lambda_{0.25}}$	-20	50	0.25	50	2

local deformations using a digital image correlation (DIC) system (Q-400 2 × 12MPixel LIMESSE GmbH, Krefeld, Germany) with a frequency of 1 Hz. The associated DIC software (Instra 4D v4.6, Dantec Dynamics A/S, Skovunde, Denmark) was then employed to construct the full-field maps of the principal strains in the centermost unit cell of each specimen. We also utilized digital extensometers to measure the longitudinal ( $\epsilon_L$ ) and transverse ( $\epsilon_T$ ) strains of these unit cells throughout the tests. Subsequently, we used a MATLAB script to calculate the true stresses ( $\sigma = f/A_0 \exp(\epsilon_L)$ ,  $A_0 = 325.12 \text{ mm}^2$ ), Poisson's ratios ( $\nu = -\epsilon_T/\epsilon_L$ , measured at 0.25 % longitudinal strain), elastic moduli ( $E$ , the slope of a line fitted between 0.1 % and 0.25 % strain of the  $\sigma - \epsilon_L$  curve), and the ultimate tensile strength ( $\sigma_{UTS}$ , the maximum recorded stress) of all the specimens. Finally, we obtained the coefficients of determination ( $R^2$ ) between the experimental and computational results to quantify the correlation between both types of results.

### 3. Results and discussion

#### 3.1. Performance of the remodeling process

Subjecting the initial unit cell designs to the adaptations of the remodeling process led to the emergence of a myriad of unit cells and provided a more extensive design space than the initial quasi-random designs (Fig. 2 and Figure S3 of the supplementary document). For every  $\rho$ ,  $\lambda$ , and  $\theta$  combination, each remodeling iteration resulted in a unique arrangement of hard and soft voxels. These unique arrangements gave rise to emergent geometrical features with an intermediate length scale between those of the unit cells and voxels. These features, although not directly linked to the auxeticity of the structure, are linked to the initial design of the lattices, with the rearrangement depending on the regions where stress concentrations were most present. The type of the emergent feature reflected the bias towards either one of the loading directions as specified by  $\lambda$  (Fig. 2A). For example, selecting  $\lambda = 0$  led to hard material distributions in the shape of parallel fibers along direction 2 for both auxetic and non-auxetic structures. The emergence of such features is expected because  $\mathbf{S}$  solely depends on the loading along direction 2, leading to a highly anisotropic unit cell (Fig. 2B). Conversely,  $\lambda = 1$  resulted in concentrations of hard material around the lattice corners with acute angles and along the edges of their opposing ends. These types of emergent 'lattice-within-lattice' arrangements were responsible for increasing the flexural rigidity of the struts, thereby enhancing the structural stiffness along direction 1. A combination of these two remarkable design features emerged for intermediate  $\lambda$  values. Moreover, the emergence of these design features took place regardless of  $\rho$  (Figure S3A of the supplementary document), indicating the consistency of the obtained computational results and supporting the conclusion that such design features can be used for the adjustment of the anisotropic properties of (hierarchical) lattice structures. This is similar to how the bone microarchitecture adapts to the applied loads to create a specific (anisotropic) orientation toward that specific loading direction.

The wide range of the emergent features also meant that the envelope of the achievable elastic properties was considerably expanded (Fig. 2B, Figure S3B of the supplementary document). More specifically, the properties varied anisotropically and corresponded to  $\lambda$ . After remodeling, the models processed with a  $\lambda$  value of 1 increased  $E_{11}$  (*e.g.*, by 12.4 % and 22 % for  $\rho = 50\%$ ,  $\theta = -20^\circ$  and  $20^\circ$ , respectively) while reducing  $E_{22}$ . For  $\lambda = 0$ ,  $E_{22}$  increased regardless of the  $\rho$  value (*e.g.*, by 73.9 % and 48.6 % for  $\rho = 50\%$ ,  $\theta = -20^\circ$  and  $20^\circ$ , respectively), while  $E_{11}$  dropped to near-zero values. Moreover, for these extreme scenarios, the process minimally affected the Poisson's ratio along the preferred remodeling direction (*i.e.*,  $\nu_{12}$  and  $\nu_{21}$  for  $\lambda = 1$  and  $\lambda = 0$ , respectively) while these converged to zero in the orthogonal direction. A mixture of these property enhancements or reductions existed for the intermediate values of  $\lambda$ . As expected, the most isotropic changes of elastic behavior were achieved when  $\lambda = 0.5$ .

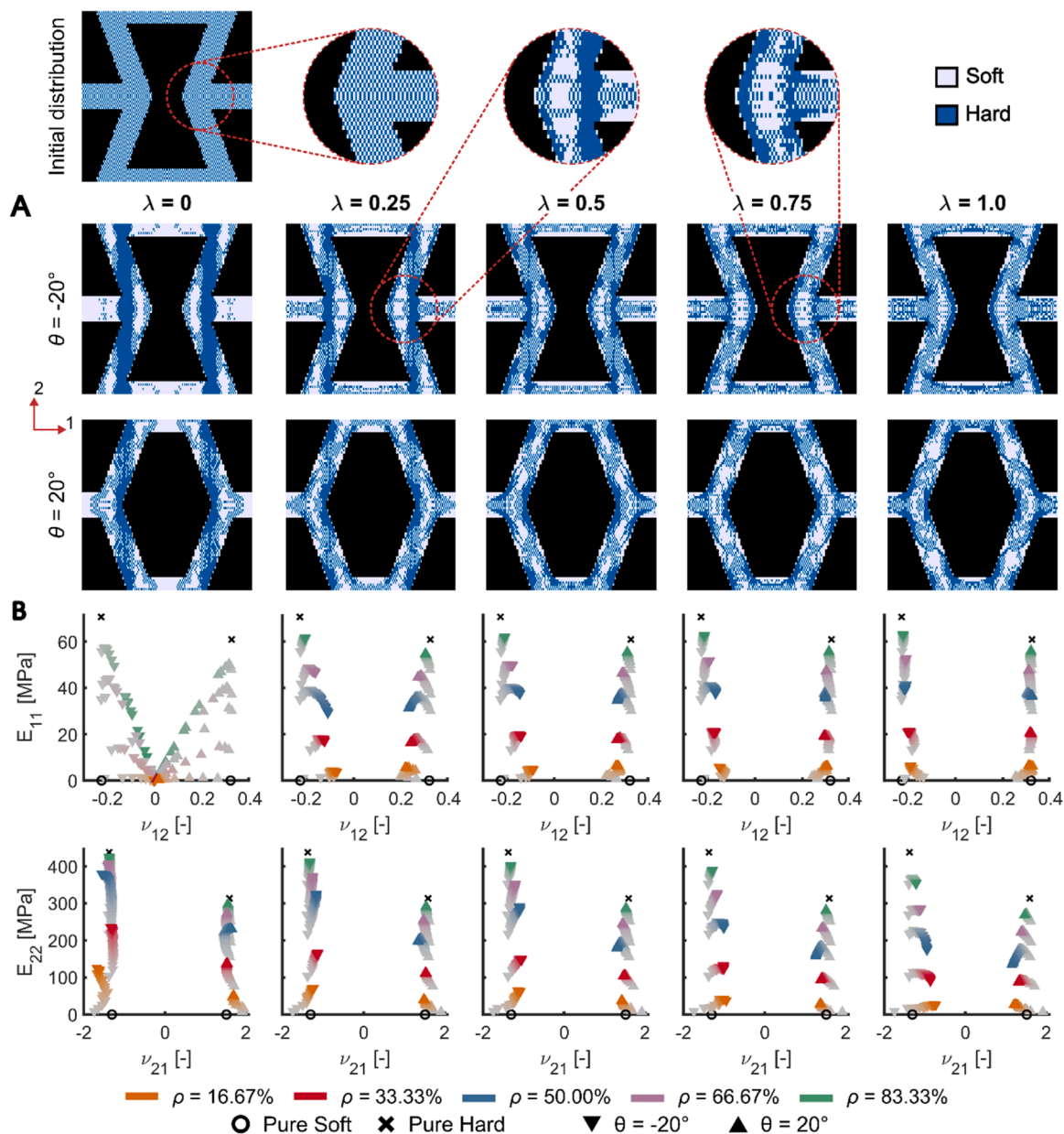


**Fig. 2.** A) The hierarchical features with an intermediate length scale, which emerged from the application of the remodeling algorithm for the specimens with 50 % hard voxels. B) These features resulted in the expansion of the envelope of the achievable elastic properties. The parameter  $\lambda$  determines the bias of the remodeling algorithm towards loading along direction 1 (*i.e.*,  $\lambda = 1$ ) or direction 2 (*i.e.*,  $\lambda = 0$ ). The grey-to-colored scale represents the initial to final remodeling iterations, respectively.

We then examined the effects of applying the bone-mimicking optimization process on the redistribution of SED to study whether the applied design methodology attenuates the stress concentrations present in the re-entrant and honeycomb unit cells. Before remodeling, the representative auxetic design (*i.e.*,  $\lambda = 0.5$ ,  $\rho = 50\%$ ) presented high degrees of strain energy concentration in the areas close to the strut corners for both types of loading directions (Fig. 3A). These peaks were within the hard voxels and, regardless of  $\lambda$ , were attenuated within the initial iterations (Fig. 3B-D). Although the soft voxels generally showed increasing energy peaks as the remodeling process progressed (particularly when loaded along direction 1), the magnitudes of these peaks were lower than those of the hard voxels by one order of magnitude. After remodeling, substantial energy peaks were only present when the highly anisotropic designs were loaded orthogonal to their intended loading direction (*i.e.*, direction 1 for  $\lambda = 0$  and direction 2 for  $\lambda = 1$ ) (Figure S4B-C of the supplementary document). For the remaining cases,

the features introduced by the optimizations resulted in more homogeneous energy distributions (Supplementary videos 1–6, Figure S4D of the supplementary document). Furthermore, the total SED plots (Figure S4E of the supplementary document) indicated that additional energy increasingly accumulated within the unit cells along their preferred remodeling direction, explaining their general stiffening. These phenomena indicate that the remodeling algorithm promotes a synergistic arrangement of the hard and soft voxels to improve the mechanical response of the unit cells, which we further validated with experiments. Interestingly, these emergent features resemble those determined parametrically in other works [52–54] wherein allocating the softer phase to hinges generally led to improved overall performance, decoupling of properties, and an expansion of the available design space. When compared with previously reported results, the advantage of our approach is that it is algorithmic and, thus, automated, leading to more complex microarchitectures which can then be realized

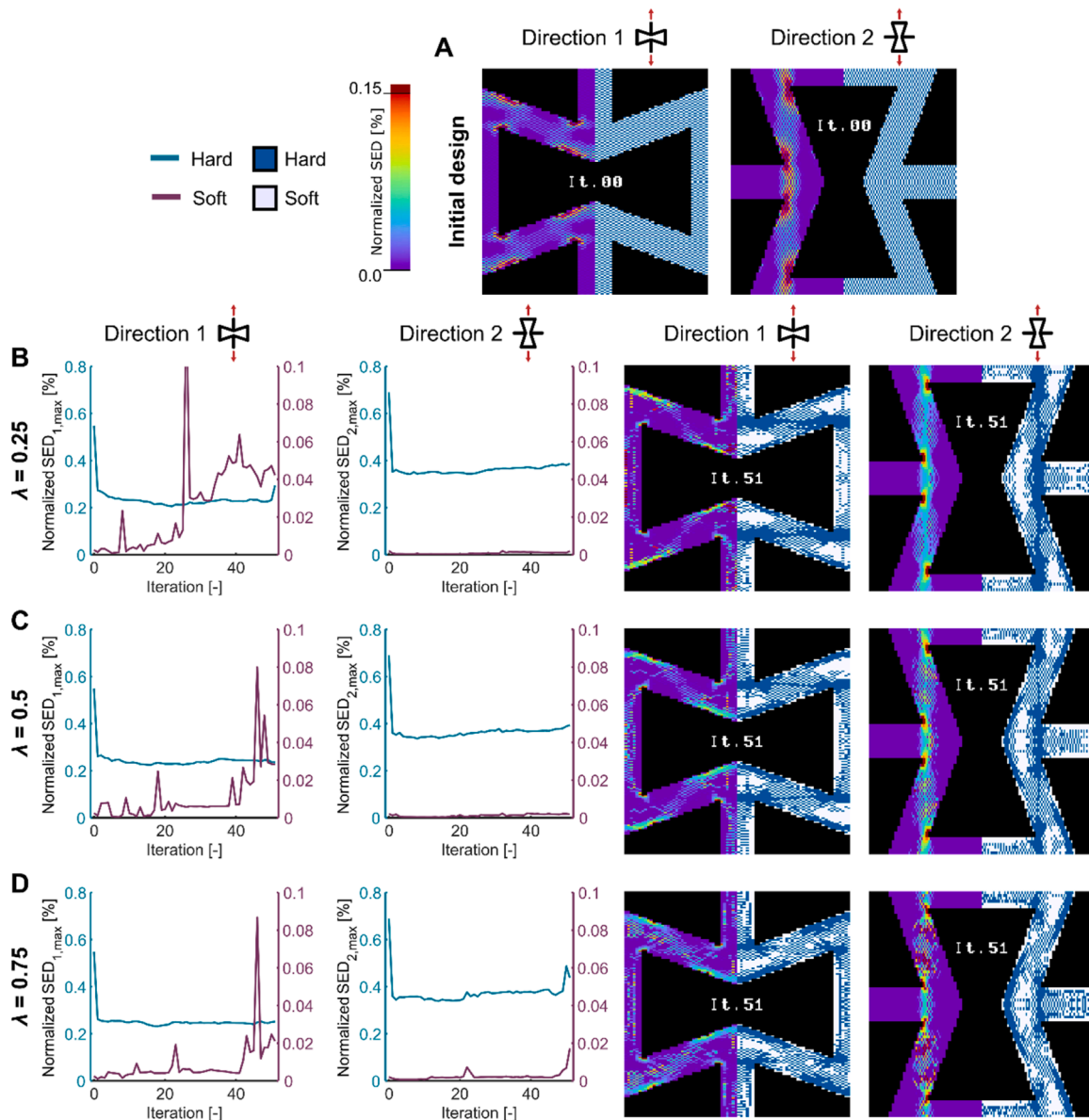


**Fig. 3.** A) The normalized SED values of the initial quasi-random bitmap designs when loaded in tension along both orthogonal directions. As the remodeling process progressed, an intermediate length scale emerged while the peaks and distributions of normalized SED adjusted: B)  $\lambda = 0.25$ , C)  $\lambda = 0.5$ , and D)  $\lambda = 0.75$ .

at the microscale using voxel-based multi-material printing. This also enables anisotropy adjustment for application-specific purposes.

### 3.2. Experimental validation

The auxetic monolithically hard lattices, which were designed as controls, exhibited a linear elastic behavior followed by brittle failure (Fig. 4A, and Table S1 of the supplementary document). In contrast, all the quasi-random initial bitmap designs had a nonlinear response and presented a stress-softening behavior, indicating that plastic deformations were present. The designs that resulted from remodeling showed a similar response. However, their response was stiffer, and their ultimate tensile stress ( $\sigma_{UTS}$ ) was higher for all the considered cases (Table S1 of the supplementary document). In fact, for the tested designs,  $\sigma_{UTS}$  was up to 1.78 times higher along direction 1 (i.e.,  $E_{1,max,\lambda_{0.75}}$ ) and up to 1.77 times stronger along direction 2 (i.e.,  $E_{2,max,\lambda_{0.25}}$ ). Similarly, the elastic modulus was up to 1.8 (i.e.,  $E_{1,max,\lambda_{0.75}}$ ) and 3.67 (i.e.,  $E_{1,max,\lambda_{0.75}}$ ) times higher along directions 1 and 2, respectively (see Supplementary videos 1–6). These drastic improvements in the

mechanical behavior of the specimens demonstrate that the remodeling algorithm can substantially enhance the properties of the initial sub-optimal designs.

It is important to note that the small standard deviations observed in our measurements demonstrate the repeatability and reproducibility of our experimental procedures. More specifically, for the elastic moduli, the coefficient of variation (CV) for monolithically hard lattices in directions 1 and 2 was 3.10 % and 2.31 %, respectively. The maximum CV values observed were 11 % for the elastic moduli of composite structures in direction 2 (initial) and direction 1 (with  $\lambda = 0.75$ ). For the other composites, these values were lower (Table S1 of the supplementary document). Similarly, a CV of <9 % was observed for the maximum strength values from quasi-static tensile tests of both optimized and initial composite lattice structures (Table S1 of the supplementary document).

A one-to-one comparison analysis between the measured and the FEM-predicted mechanical properties indicated that the FEM models can accurately predict the mechanical properties of the specimens (i.e.,  $R^2_{E,1:1} = 86.3$  % for the elastic moduli,  $R^2_{\nu,1:1} = 94.31$  % for the Poisson's

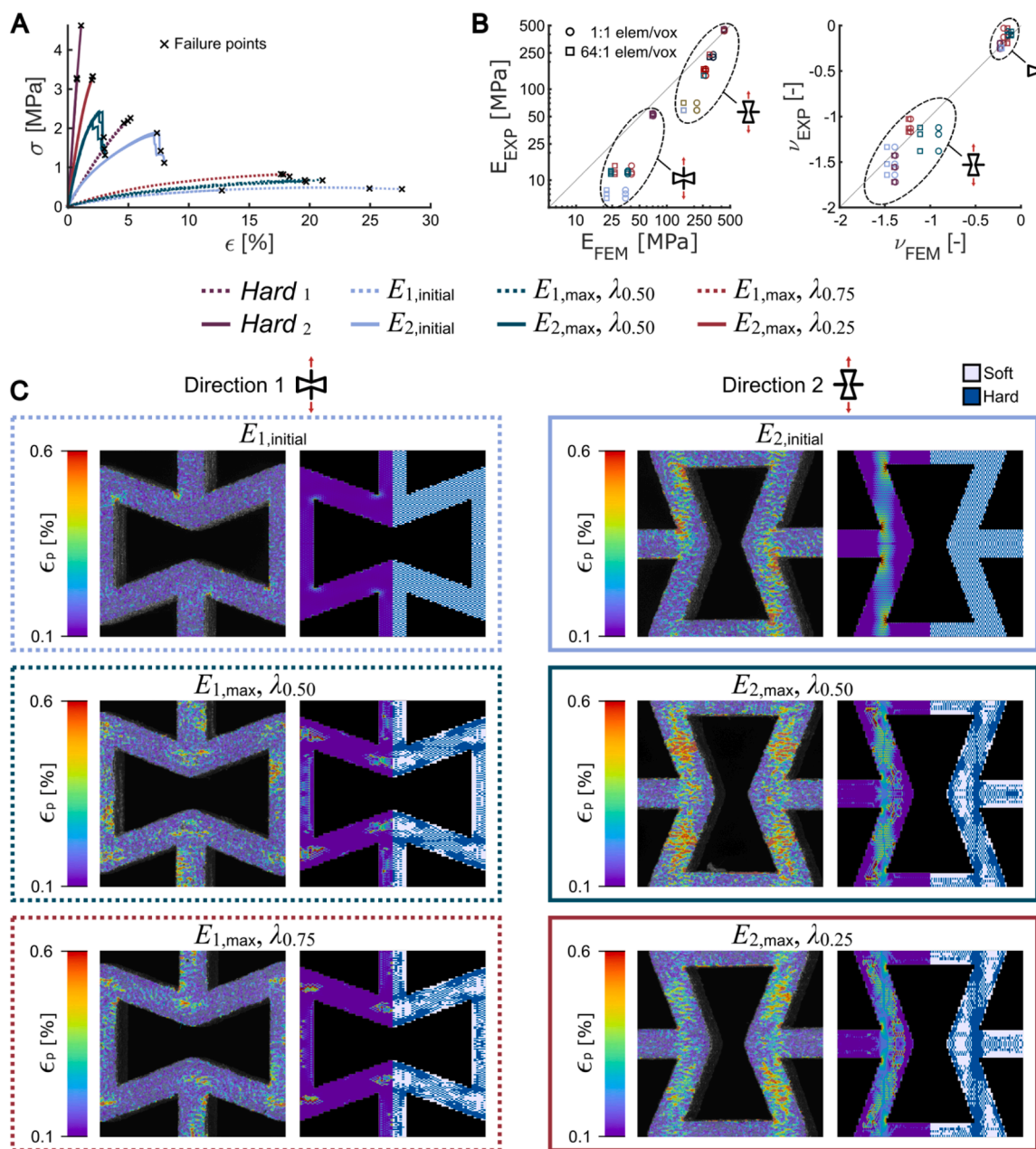


**Fig. 4.** A) The stress-strain curves corresponding to the validation tests performed on a selected number of designs with 50 % hard voxels. B) The experimental vs. simulation results for the elastic modulus ( $E$ ) and Poisson's ratio ( $\nu$ ) for two different numbers of elements per voxel (*i.e.*, 1:1 and 64:1). C) The distribution of the first true principal strain ( $\epsilon_p$ ) as measured by DIC and as predicted by our FEM models (tensile strain = 0.25 %).

ratios, Fig. 4B). The elastic moduli of the control group (*i.e.*, monolithically hard lattices) were predicted most accurately, while those of the bitmap designs were overestimated. These discrepancies were due to the alternating material nature within the bitmap unit cells, material mixing effects, size effects due to the lack of complete periodicity of the lattice structures, and inaccuracies inherent in DIC measurements, particularly at lower strains, which are known to result in stiffness overestimations [44,56]. We accounted for this artifact by increasing the FEM element to voxel representation from 1:1 to 64:1, which improved the accuracy of the validation simulations, particularly for the elastic modulus (*i.e.*,  $R_{E,64:1}^2 = 91.85\%$ ,  $R_{\nu,64:1}^2 = 96.5\%$ ). However, this improved accuracy came with an exponential increase in the CPU time (Figure S2B of the supplementary document), which made performing the remodeling analysis at such representation unfeasible. The improvements in the mechanical properties remained consistent and, in

fact, even improved upon using higher element-to-voxel ratios. The emergent design features were also consistent between both levels of discretization. Moreover, the Poisson's ratios were captured highly accurately even when the smaller number of elements per voxel (*i.e.*, 1:1) was used. We, therefore, concluded that a 1:1 element-to-voxel ratio was sufficient for running the bone-mimicking design optimization routine. Once the optimal design is found, one can use a higher element-to-voxel ratio to capture the elastic properties of the resulting designs more accurately. Another option would be to run a few additional steps of design optimization starting from the design resulting from the lower ratio simulations (Figure S2F of the supplementary document).

When comparing the FEM-predicted strain distribution with the full-field strain measurements performed using DIC respectively (see Supplementary videos 1–6), we found that the simulations captured the

most important features of the experimentally observed deformation patterns (Fig. 4C). For the initial quasi-random designs, we observed peaks of strains at the hinge locations of the specimens and a relatively homogeneous distribution of lower strain values throughout the unit cell. These distributions explain the lower maximum stress and elastic moduli of the initial designs. The strain distributions of the remodeled designs were generally more homogeneous in both the simulations and experiments. Both of the designs that resulted from the application of the optimization algorithm to loading along direction 1 (i.e.,  $E_{1,max}$ ,  $\lambda_{0.50}$  and  $E_{1,max}$ ,  $\lambda_{0.75}$ ) concentrated the strains around the strut intersections and along the struts parallel to the loading direction, which is similar to the FEM predictions. Similarly, the designs that were optimized for loading along direction 2 (i.e.,  $E_{2,max}$ ,  $\lambda_{0.50}$  and  $E_{2,max}$ ,  $\lambda_{0.25}$ ) led to increased strains within the diagonal struts, with relatively higher strains present in the experiments than in the simulations. These more homogeneous strain distributions confirm the success of the proposed bone-mimicking design algorithm in improving the utilization of the available hard and soft voxels through the emergence of geometrical features at an intermediate length scale between the unit cell and voxel dimensions.

Our previous results [44,56,58] indicate that while blending does contribute to enhanced toughness by mitigating stress concentrations at the interface, the overall geometrical structure plays a more dominant role in determining mechanical performance. Particularly, when voxels of the same material (either hard or soft) are adjacent, the structure behaves more homogeneously within that material phase. However, when hard and soft voxels are neighboring, the interface introduces localized stress variations, which can influence deformation patterns, energy dissipation, and failure mechanisms.

By incorporating a biomimetic remodeling process, we used these interactions to optimize the internal architecture of the metamaterials, ensuring that hard-soft transitions occur in a way that enhances mechanical efficiency instead of becoming failure-prone regions.

To further extend our understanding of the influence of optimizations in directions 1 and 2 on other mechanical properties of these lattice structures, we measured the toughness (i.e., the area below the stress-strain curves until the rupture point) and resilience (i.e., the energy absorbed until maximum stress was reached) properties of these lattices (Figure S5 of the supplementary document). This comparison showed a notable increase in both resilience and toughness of the lattices optimized in direction 1 in comparison to the initial state (Figure S5B of the supplementary document). This enhancement, however, was not observed in the optimizations performed in direction 2, indicating a distinct response based on the direction of optimization (Figure S5B of the supplementary document). Interestingly, the toughness of the composite lattice structure can surpass the properties of the single-lattice structures for both loading directions independent from the hard volume fraction (Figure S5B of the supplementary document).

We need to emphasize here that unlike traditional topology optimization (TO) methods that rely on a global cost function, our remodeling algorithm operates through an iterative material redistribution process inspired by bone adaptation, which is local in nature. This approach does not look for a single global optimum but rather evolves the internal architecture of the metamaterial in response to local mechanical cues. Voxels are progressively assigned to either the hard or soft phase during each iteration based on their SED, ensuring that mechanically meaningful structures emerge. Because this process continuously adapts to local conditions rather than attempting to minimize or maximize a predefined objective function, issues related to non-convergence or entrapment in local optima are not applicable. Moreover, while different initial conditions may lead to variations in the final structure, this is an expected and desirable outcome, as it reflects the adaptability of the remodeling process rather than a failure to achieve an optimal configuration. This feature makes the method particularly robust for designing stress-worthy hierarchical metamaterials with tunable mechanical properties (see Section 3.3).

### 3.3. Extension of the design approach to other unit cell geometries

We extended the analysis and our design approach to include two additional unit cell shapes (i.e., the tetra-anti-chiral [59] (Fig. 5a) and the 2D equivalent of a hexaround [60] (Fig. 5b)) to determine if a similar trend can be observed. This further analysis revealed that similar features, particularly the reduction of strain concentration peaks and the homogenization of SED fields, were also present in these types of lattices (Fig. 5). The unique microarchitectural features also began to emerge from those regions depending on the applied loading directions (Fig. 5c). Furthermore, the expansion of the property design space observed for these structures aligned with the patterns identified in the initial (non-) auxetic lattices. These findings suggested that the beneficial effects observed in the initially studied (i.e., re-entrant and honeycomb) unit cells were not unique to those geometries but could also be observed in a broader range of lattice configurations. Therefore, the rational design of unit cell geometries can effectively influence the mechanical performance of multi-material metamaterial lattice structures and eventually contribute to their final microarchitectural designs.

### 3.4. Use of another theoretical models to simulate the bone-remodeling process

We expanded our analyses to investigate the characteristics of lattice structures through the application of a more sophisticated and recent bone remodeling algorithm, as detailed in [34]. This advanced algorithm, which incorporates the metabolic effects of bone into modeling efforts, was adapted in our research to predominantly focus on the mechanical loading aspects of the bone adaptation process. Notably, this algorithm extends beyond the conventional assessment of SED at a singular voxel level by also considering the SED from the immediate surrounding neighborhood. This comprehensive approach facilitates a deeper understanding of the influence of mechanical loading on the bone remodeling process, yielding insights crucial for creating more precise models in bone research and the associated domains.

Our motivation for adopting this algorithm stemmed from its ability to capture some of the more intricate aspects of the bone tissue adaptation process as well as its novelty for the design of voxel-based, multi-material metamaterials. The algorithm's utility in our study lies in its ability to capture the SED not just of the local voxel but also of its surrounding environment, a feature critical for accurately simulating the mechanical behavior of bone under various loading conditions. This aspect was particularly relevant for the development of models within multi-material and voxel-based frameworks, where complexity and material heterogeneity play significant roles.

The specific equations guiding this algorithmic approach are detailed in what follows. The algorithm updated the conventional  $SED_1$  and  $SED_2$  terms in the calculation of the min-max scaled  $U_1$  and  $U_2$  terms of Eq. (1), replacing them with  $Sr_1$  and  $Sr_2$ . These terms represent the mechanical signal ratios of each element within the lattice under two distinct loading directions, calculated as  $Sr_1 = (SED_1)/(Sd_1)$  and  $Sr_2 = (SED_2)/(Sd_2)$ , with  $Sd_1 = (\int_{\Omega} SED_1 w(l) d\Omega) / (\int_{\Omega} w(l) d\Omega)$  and  $Sd_2 = (\int_{\Omega} SED_2 w(l) d\Omega) / (\int_{\Omega} w(l) d\Omega)$ , where  $Sd_1$  and  $Sd_2$  denote the neighboring mechanical states integrated over the communication region  $\Omega$  of each lattice element.

The weight function  $w(l)$  describes how the signal decays relative to the distance between the reference element of  $\Omega$  and each of the neighboring ones, which is defined as:

$$w(l) = |1 - l/l_m| \text{ for } l < l_m \text{ and } w(l) = 0 \text{ for } l \geq l_m$$

with  $l_m$  being the maximum distance of the  $\Omega$  region.

In applying these equations, we conducted simulations with a characteristic distance ( $l_m$ ) set to 20 voxels for directions 1 and 2, and 4 voxels for direction 3, which corresponds to the entire depth of the unit

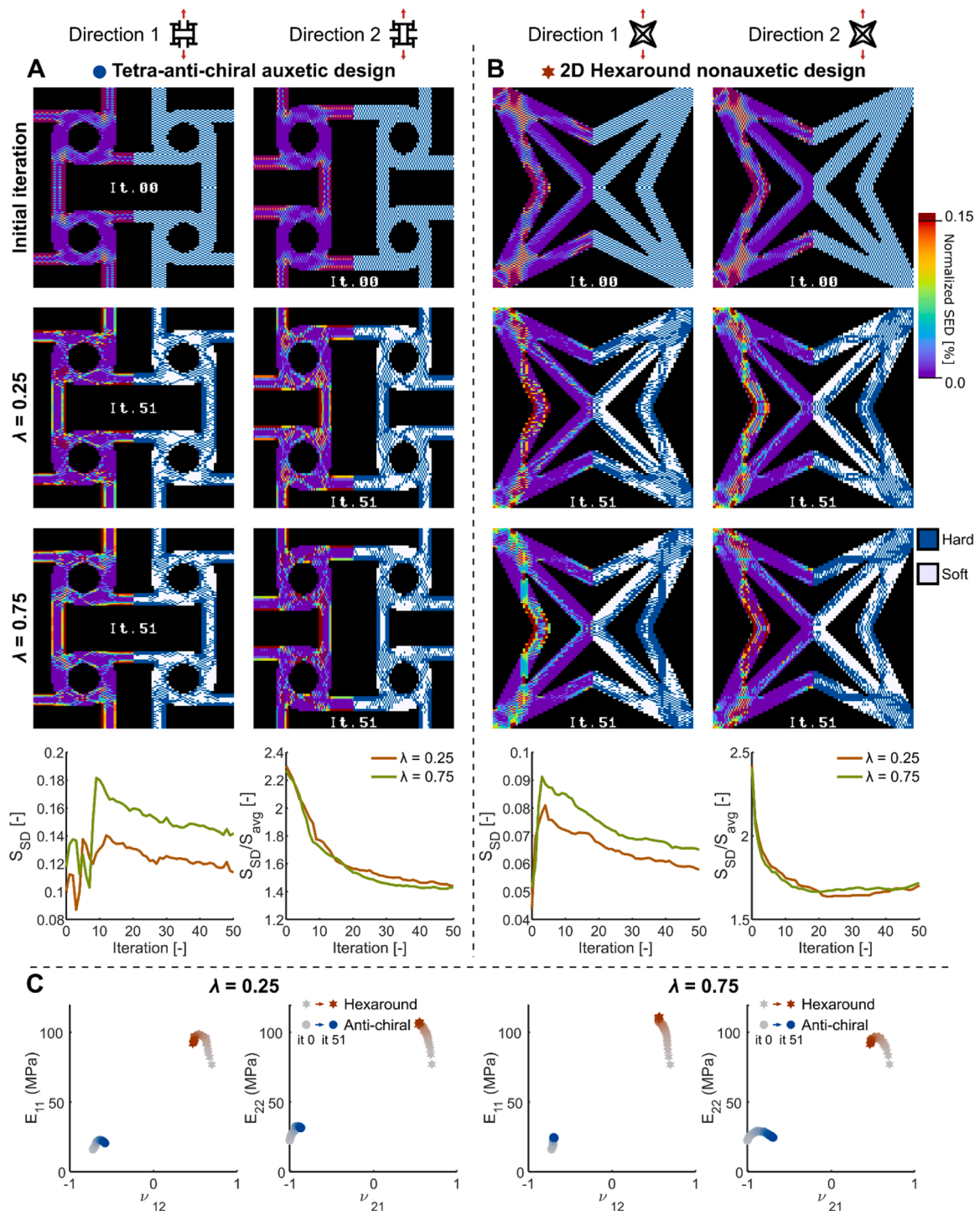


**Fig. 5.** The results of applying the bone remodeling algorithm to two different unit cell lattices, including tetra-anti-chiral (A) and hexaround (B) lattice structures and the resulting microarchitectures under two values of  $\lambda$ , namely 0.25 and 0.75. Depending on the loading direction (*i.e.*, 1 or 2), the values of the elastic moduli as well as the values of the Poisson's ratio can change during the optimization process for both auxetic (*i.e.*, tetra-anti-chiral) and non-auxetic (*i.e.*, hexaround) structures (C).

cells. These parameters were employed in the FE simulations of both auxetic and non-auxetic lattices at a 1:1 representation scale, with a relative density ( $\rho$ ) of 50 %, and a  $\lambda$  value of 0.25 and 0.75.

The outcomes of these simulations were comparable to those observed using the original algorithm, showcasing similar patterns in the minimization and homogenization of *SED* across the lattice structures. This indicates that the initially explored simplified algorithm's principles can be effectively extended to accommodate the complexities

introduced by more advanced algorithms (Fig. 6).

### 3.5. Potential applications for meta-implant design

The proposed design approach has potential applications in the design and fabrication of orthopedic medical devices. This technique allows us to expand the design space of mechanical metamaterial lattice structures solely by modifying material arrangement at another scale

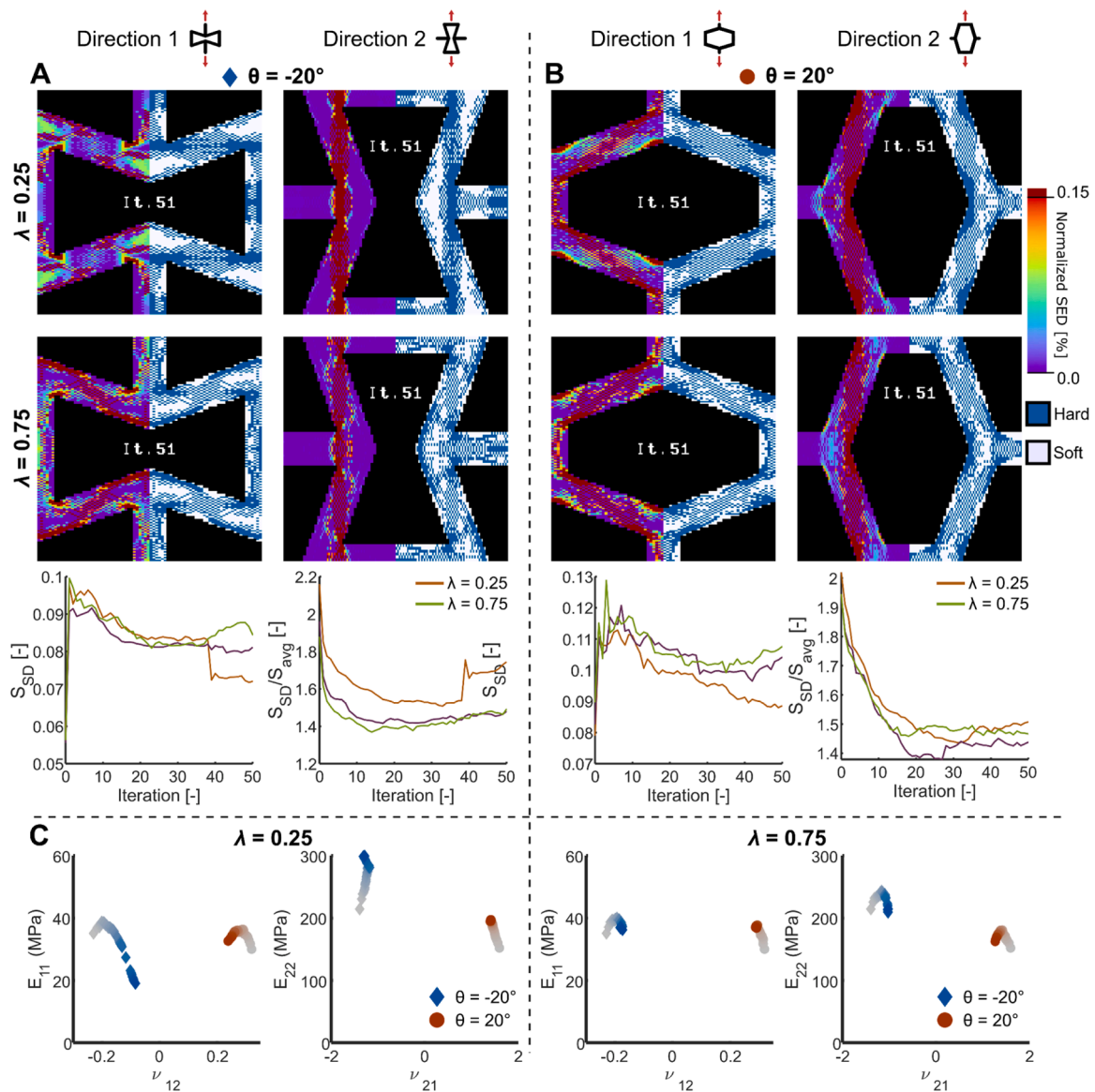


Fig. 6. Similar emerging features appeared when using another bone remodeling optimization algorithm for  $\lambda = 0.25$  and  $0.75$  for auxetic (A) and non-auxetic (B) lattice structures. These features resulted in the expansion of the envelope of the achievable elastic properties when  $\lambda = 0.25$  and  $0.75$  (C).

without modifying the geometry of a unit cell itself, thereby retaining its geometry-related benefits (e.g., mass transport characteristics). This helps to tailor the overall multi-physics properties of the metamaterials at a larger scale to meet specific needs, which is of particular interest in biomedical engineering (e.g., the trade-off between extreme Poisson's ratios, high elastic moduli, as well as high porosities and high permeability).

We have applied the design concepts proposed in this study to the rational design of multi-material meta-implants (Fig. 7). These meta-implants were created from a combination of auxetic and non-auxetic unit cells. The segment of the meta-implant consists of auxetic lattices designed to undergo tension, whereas the portion made up of non-auxetic unit cells is subjected to compression. Rationally placing these two types of unit cells enables the meta-implant to closely interact with the bone, fostering an enhanced bone-implant interface and connection. This approach has been previously suggested [13], and it is hypothesized that such a combination could significantly improve bone-implant fixation, thereby mitigating the risk of bone loosening over time.

Using the voxel-based methodology allows us to further refine the local mechanical properties of these previously developed design con-

cepts, ensuring they more closely mimic the mechanical properties of different regions of the femur bone. This includes deploying specific functions to modulate the elastic modulus in the second principal direction,  $E_{22}$ , along the implant's longitudinal axis, achieving a higher  $E_{22}$  near the femoral head which then gradually diminishes towards the distal region. In addition, to address the anisotropy of the design, we also defined a transverse elastic modulus function based on the  $E_{11}$  values of the lattices (Fig. 7B). This approach guarantees a lower elastic modulus in the regions directly contacting the bone, which subsequently increases towards the center of the stem. Such a combination of material properties is expected to stimulate improved osseointegration at the interface of the bone and the implant while also ensuring the structural integrity of the implant. Moreover, by precisely defining these mechanical properties, one can accurately align the most appropriate unit cell with the required mechanical properties for each segment of the implant. This methodology is streamlined by the uniform overall geometry of all lattices, enabling the creation of an implant that not only maintains constant mass transport properties but also displays highly heterogeneous and anisotropic properties across its structure. Thus, this conceptual design can be further combined with physics-informed

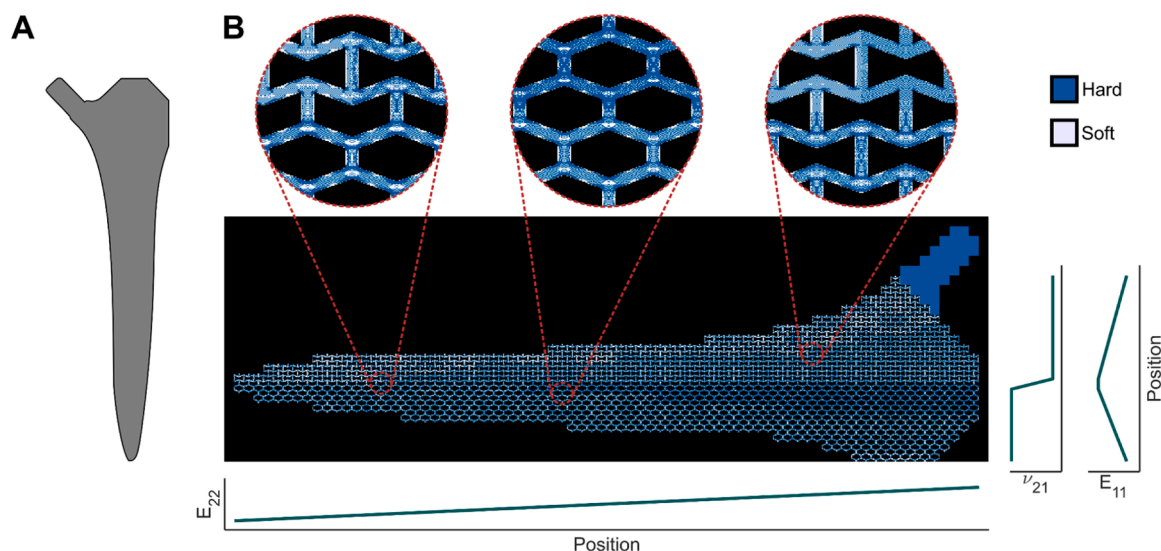


**Fig. 7.** A conceptual design for a hip implant (A) in which auxetic and non-auxetic unit cells with different hard volume fractions and microarchitectural features were tessellated within the implant design space to satisfy certain elastic properties.

models to not only match the local properties of the bone but also perfectly follow the inner contour of the bone.

This proposed design approach can, therefore, be applied to the rational design of metamaterials with enhanced load-bearing capabilities and longer service lives. The combination of unusual elastic properties and stress-worthiness offered by such designs would allow for the development of metamaterial-based devices, such as implantable medical devices [13], soft robots [61], and soft digital logic mechanisms for control and actuation [62,63].

Our remodeling algorithm inherently operates in three dimensions, enabling the rational distribution of soft and hard voxels throughout the entire volume of the structure. This ensures that material redistribution occurs along all spatial directions, including perpendicular to the fabrication plane. While this study primarily focuses on the generated sub-structures from an in-plane perspective, the same principles apply when density varies laterally or through the thickness of the metamaterial. We need to highlight here that the figures primarily depict in-plane variations for clarity, but the remodeling process itself is fully 3D, with voxels distributed across all layers.

A key advantage of our method is that, for a given material, it allows for fine-tuning of mechanical properties within a given micro-architecture to maintain the Poisson's ratio while rationally distributing soft and hard phases at the voxel level to maximize the uniformity of strain energy distribution. This helps to mitigate stress concentrations that could otherwise lead to premature failure, thereby improving the overall durability and mechanical efficiency of the structure.

By modifying initial conditions, such as the starting voxel arrangement or the applied boundary conditions, the remodeling algorithm can be adapted to generate functionally graded structures with tailored mechanical properties in different spatial regions. This capability is particularly relevant for applications requiring anisotropic mechanical responses or optimized stress distribution across varying depth profiles. While this study focuses on structures designed for in-plane loading, future work could extend the remodeling approach to account for out-of-plane forces, further refining stress distributions and enhancing mechanical performance in more complex loading scenarios. Furthermore, our simulations confirm that the emergent hierarchical features remain robust even when different material volume fractions or directional biases are introduced, confirming the versatility of this biomimetic approach for fully 3D applications.

Currently, voxel-based printing is exclusively achievable using PolyJet technology, which restricts its direct implementation in FDM-

printed metamaterials. However, despite differences in material deposition techniques, the core principles of our geometrically optimized structures remain applicable. Our simulations demonstrate that the emergent structural features generated by our biomimetic remodeling algorithm can enhance mechanical performance, even when material systems or manufacturing processes differ. Therefore, future advancements in FDM or hybrid printing technologies could facilitate the adaptation of our approach to a wider range of applications [64,65].

#### 4. Conclusions

We mimicked bone remodeling process through the introduction of a remodeling-inspired algorithm that rationally distributes hard and soft voxels within the unit cells of mechanical metamaterials. There are, therefore, two length scales that are introduced to the algorithm (*i.e.*, the length scales corresponding to the unit cell dimensions and voxel size). A third, intermediate length scale then emerges from the application of the proposed algorithm. This leads to the formation of design features that eventually lead to the expansion of the envelope of the achievable elastic properties, attenuation of the stress peaks responsible for crack initiation and growth, as well as improved failure properties and, thus, stressworthiness of the mechanical metamaterials. The parameters of the remodeling algorithm, including the one determining the bias towards a specific loading direction, determine the isotropic or anisotropic nature of the obtained mechanical properties. One could, therefore, be biased towards a specific loading direction while limiting the available material budget (*e.g.*, by limiting the number of (hard) voxels) to create highly efficient structures that can carry the intended loads with the minimum weight. The experimental validations demonstrate the accuracy of the computational models while also revealing improvements in ultimate tensile strength. Further work should, therefore, seek to augment our computational models to investigate the generated designs more efficiently. Both the proposed approach and the emergent design features could be applied to the design of multiple types of devices in various high-added-value industries, including medicine, soft robotics, and beyond.

#### CRediT authorship contribution statement

**M.C. Saldívar:** Writing – original draft, Visualization, Methodology, Investigation, Formal analysis, Conceptualization. **E. Tay:** Writing – original draft, Visualization, Validation, Methodology, Investigation,

Formal analysis, Conceptualization. **H. Pahlavani:** Writing – review & editing, Investigation, Formal analysis. **E.L. Doubrovski:** Writing – review & editing, Supervision, Software, Formal analysis. **M.J. Mirzaali:** Writing – original draft, Validation, Supervision, Resources, Project administration, Methodology, Investigation, Funding acquisition, Formal analysis, Data curation, Conceptualization. **A.A. Zadpoor:** Writing – original draft, Supervision, Software, Resources, Investigation, Funding acquisition, Conceptualization.

### Declaration of competing interest

The authors declare that they have no known competing financial interests or personal relationships that could have appeared to influence the work reported in this paper.

### Acknowledgments

This project is part of the Idea Generator (NWA-IDG) research program with code numbers NWA.1228.192.206 and NWA.1228.192.228. M. J. M. acknowledges the funding from NWO grant OCEANW.XS22.2.044. This research was conducted on a Stratasys® Objet350 Connex3™ printer through the Voxel Print Research Program. This program is an exclusive partnership with Stratasys Education that enhances the value of 3D printing as a powerful platform for experimentation, discovery, and innovation; for more information, contact: academic.research@stratasys.com.

### Supplementary materials

Supplementary material associated with this article can be found, in the online version, at [doi:10.1016/j.apmt.2025.102722](https://doi.org/10.1016/j.apmt.2025.102722).

### Data availability

Data will be made available on request.

### References

- D. Chen, X. Zheng, Multi-material additive manufacturing of metamaterials with giant, tailorable negative poisson's ratios, *Sci. Rep.* 8 (1) (2018) 9139.
- M.J. Mirzaali, S. Janbaz, M. Strano, L. Vergani, A.A. Zadpoor, Shape-matching soft mechanical metamaterials, *Sci. Rep.* 8 (1) (2018) 965.
- X. Zheng, H. Lee, T.H. Weisgraber, M. Shusteff, J. DeOtte, E.B. Duoss, J.D. Kuntz, M.M. Biener, Q. Ge, J.A. Jackson, S.O. Kucheyev, N.X. Fang, C.M. Spadaccini, Ultralight, ultrastiff mechanical metamaterials, *Science* (1979) 344 (6190) (2014) 1373–1377.
- K. Bertoldi, V. Vitelli, J. Christensen, M. van Hecke, Flexible mechanical metamaterials, *Nat. Rev. Mater.* 2 (11) (2017) 17066.
- S. Bonfanti, S. Hiemer, R. Zulkarnain, R. Guerra, M. Zaiser, S. Zapperi, Computational design of mechanical metamaterials, *Nat. Comput. Sci.* 4 (8) (2024) 574–583.
- Y. Javanmardi, H. Colin-York, N. Szita, M. Fritzsche, E. Moeendarbary, Quantifying cell-generated forces: poisson's ratio matters, *Commun. Phys.* 4 (1) (2021) 237.
- E. Yarali, A.A. Zadpoor, U. Staufner, A. Accardo, M.J. Mirzaali, Auxeticity as a mechanobiological tool to create meta-biomaterials, *ACS. Appl. Bio Mater.* (2023).
- E. Yarali, M. Klimopoulou, K. David, P.E. Boukany, U. Staufner, L.E. Fratila-Apachitei, A.A. Zadpoor, A. Accardo, M.J. Mirzaali, Bone cell response to additively manufactured 3D micro-architectures with controlled Poisson's ratio: auxetic vs. non-auxetic meta-biomaterials, *Acta Biomater.* (2024).
- Q. Shi, J. Chen, J. Chen, Y. Liu, H. Wang, Application of additively manufactured bone scaffold: a systematic review, *Biofabrication.* 16 (2) (2024) 022007.
- J.U. Surjadi, L. Gao, H. Du, X. Li, X. Xiong, N.X. Fang, Y. Lu, Mechanical metamaterials and their engineering applications, *Adv. Eng. Mater.* 21 (3) (2019) 1800864.
- J.M. Parente, P.N.B. Reis, Fatigue behaviour of 3d printed auxetic materials: an overview, *Procedia Structural Integrity* 53 (2024) 221–226.
- J.M. Parente, P.N.B. Reis, F. Berto, Fatigue response of auxetic structures: a review, *Fatigue Fract. Eng. Mater. Struct.* 47 (8) (2024) 2679–2699.
- H.M.A. Kolken, S. Janbaz, S.M.A. Leeftang, K. Liettaert, H.H. Weinans, A. A. Zadpoor, Rationally designed meta-implants: a combination of auxetic and conventional meta-biomaterials, *Mater. Horiz.* 5 (1) (2018) 28–35.
- H.M.A. Kolken, A.A. Zadpoor, Auxetic mechanical metamaterials, *RSC. Adv.* 7 (9) (2017) 5111–5129.
- M.J. Mirzaali, A.A. Zadpoor, Orthopedic meta-implants, *APL Bioeng.* 8 (1) (2024) 010901, <https://doi.org/10.1063/5.0179998>.
- A.A. Zadpoor, Mechanical meta-materials, *Mater. Horiz.* 3 (5) (2016) 371–381.
- X. Ren, R. Das, P. Tran, T.D. Ngo, Y.M. Xie, Auxetic metamaterials and structures: a review, *Smart Mater. Struct.* 27 (2) (2018) 023001.
- M.N. Andersen, F. Wang, O. Sigmund, On the competition for ultimately stiff and strong architected materials, *Mater. Des.* 198 (2021) 109356.
- M.J. Mirzaali, R. Hedayati, P. Vena, L. Vergani, M. Strano, A.A. Zadpoor, Rational design of soft mechanical metamaterials: independent tailoring of elastic properties with randomness, *Appl. Phys. Lett.* 111 (5) (2017) 051903.
- M.J. Mirzaali, H. Pahlavani, E. Yarali, A.A. Zadpoor, Non-affinity in multi-material mechanical metamaterials, *Sci. Rep.* 10 (1) (2020) 11488.
- O. Eren, H.K. Sezer, N. Yalçın, Effect of lattice design on mechanical response of PolyJet additively manufactured cellular structures, *J. Manuf. Process.* 75 (2022) 1175–1188.
- V.S. Deshpande, M.F. Ashby, N.A. Fleck, Foam topology: bending versus stretching dominated architectures, *Acta Mater.* 49 (6) (2001) 1035–1040.
- C. Zhan, M. Li, R. McCoy, L. Zhao, W. Lu, 3D printed hierarchical re-entrant honeycombs: enhanced mechanical properties and the underlying deformation mechanisms, *Compos. Struct.* 290 (2022) 115550.
- R. Gatt, M. Vella Wood, A. Gatt, F. Zarb, C. Formosa, K.M. Azzopardi, A. Casha, T. P. Agius, P. Schembri-Wismayer, L. Attard, N. Chockalingam, J.N. Grima, Negative Poisson's ratios in tendons: an unexpected mechanical response, *Acta Biomater.* 24 (2015) 201–208.
- C. Lees, J.F.V. Vincent, J.E. Hillerton, Poisson's ratio in skin, *Biomed. Mater. Eng.* 1 (1991) 19–23.
- U.G.K. Wegst, H. Bai, E. Saiz, A.P. Tomsia, R.O. Ritchie, Bioinspired structural materials, *Nat. Mater.* 14 (1) (2015) 23–36.
- W. Huang, D. Restrepo, J.-Y. Jung, F.Y. Su, Z. Liu, R.O. Ritchie, J. McKittrick, P. Zavattieri, D. Kisailus, Multiscale toughening mechanisms in biological materials and bioinspired designs, *Advanced Materials* 31 (43) (2019) 1901561.
- M. Grossman, D. Pivovarov, F. Bouville, C. Dransfeld, K. Masania, A.R. Studart, Hierarchical toughening of Nacre-like composites, *Adv. Funct. Mater.* 29 (9) (2019) 1806800.
- S.E. Naleway, M.M. Porter, J. McKittrick, M.A. Meyers, Structural design elements in biological materials: application to bioinspiration, *Advanced Materials* 27 (37) (2015) 5455–5476.
- J.W.C. Dunlop, P. Fratzl, Biological composites, *Annu Rev. Mater. Res.* 40 (1) (2010) 1–24.
- D. Sen, M.J. Buehler, Structural hierarchies define toughness and defect-tolerance despite simple and mechanically inferior brittle building blocks, *Sci. Rep.* 1 (1) (2011) 35.
- R. Huiskes, R. Ruimerman, G.H. van Lenthe, J.D. Janssen, Effects of mechanical forces on maintenance and adaptation of form in trabecular bone, *Nature* 405 (6787) (2000) 704–706.
- R. Huiskes, H. Weinans, H.J. Grootenboer, M. Dalstra, B. Fudala, T.J. Slooff, Adaptive bone-remodeling theory applied to prosthetic-design analysis, *J. Biomech.* 20 (11) (1987) 1135–1150.
- Y. Kameo, Y. Miya, M. Hayashi, T. Nakashima, T. Adachi, In silico experiments of bone remodeling explore metabolic diseases and their drug treatment, *Sci. Adv.* 6 (10) (2020) eaax0938.
- M.M.A. Peyroteo, J. Belinha, L.M.J.S. Dinis, R.M.N. Jorge, Bone remodeling: an improved spatiotemporal mathematical model, *Arch. Appl. Mech.* 90 (3) (2020) 635–649.
- C. Ruff, B. Holt, E. Trinkaus, Who's afraid of the big bad Wolff? "Wolff's law" and bone functional adaptation, *Am. J. Phys. Anthropol.* 129 (4) (2006) 484–498.
- G. Campoli, H. Weinans, F. van der Helm, A.A. Zadpoor, Subject-specific modeling of the scapula bone tissue adaptation, *J. Biomech.* 46 (14) (2013) 2434–2441.
- G. Campoli, H. Weinans, A.A. Zadpoor, Computational load estimation of the femur, *J. Mech. Behav. Biomed. Mater.* 10 (2012) 108–119.
- P. Christen, K. Ito, R. Müller, M.R. Rubin, D.W. Dempster, J.P. Bilezikian, B. van Rietbergen, Patient-specific bone modelling and remodelling simulation of hypoparathyroidism based on human iliac crest biopsies, *J. Biomech.* 45 (14) (2012) 2411–2416.
- P. Christen, B. van Rietbergen, F.M. Lambers, R. Müller, K. Ito, Bone morphology allows estimation of loading history in a murine model of bone adaptation, *Biomech. Model. Mechanobiol.* 11 (3) (2012) 483–492.
- H. Weinans, R. Huiskes, H.J. Grootenboer, The behavior of adaptive bone-remodeling simulation models, *J. Biomech.* 25 (12) (1992) 1425–1441.
- K.-i. Tsubota, T. Adachi, Y. Tomita, Functional adaptation of cancellous bone in human proximal femur predicted by trabecular surface remodeling simulation toward uniform stress state, *J. Biomech.* 35 (12) (2002) 1541–1551.
- I. Giorgio, M. Spagnuolo, U. Andreus, D. Scerrato, A.M. Bersani, In-depth gaze at the astonishing mechanical behavior of bone: a review for designing bio-inspired hierarchical metamaterials, *Math. Mech. Solids.* 26 (7) (2021) 1074–1103.
- M.C. Saldívar, E.L. Doubrovski, M.J. Mirzaali, A.A. Zadpoor, Nonlinear coarse-graining models for 3D printed multi-material biomimetic composites, *Addit. Manuf.* 58 (2022) 103062.
- M.J. Mirzaali, M. Cruz Saldívar, A. Herranz de la Nava, D. Gunashekar, M. Nouri-Goushki, E.L. Doubrovski, A.A. Zadpoor, Multi-material 3D printing of functionally graded hierarchical soft-Hard composites, *Adv. Eng. Mater.* 22 (7) (2020) 1901142.
- G.X. Gu, C.-T. Chen, D.J. Richmond, M.J. Buehler, Bioinspired hierarchical composite design using machine learning: simulation, additive manufacturing, and experiment, *Mater. Horiz.* 5 (5) (2018) 939–945.

- [47] S. Hasanov, A. Gupta, A. Nasirov, I. Fidan, Mechanical characterization of functionally graded materials produced by the fused filament fabrication process, *J. Manuf. Process.* 58 (2020) 923–935.
- [48] L. Zhu, L. Sun, X. Wang, N. Li, Optimisation of three-dimensional hierarchical structures with tailored lattice metamaterial anisotropy, *Mater. Des.* 210 (2021) 110083.
- [49] I. Kuszczak, F.I. Azam, M.A. Bessa, P.J. Tan, F. Bosi, Bayesian optimisation of hexagonal honeycomb metamaterial, *Extreme Mech. Lett.* 64 (2023) 102078.
- [50] L. Dong, D. Wang, Optimal design of three-dimensional voxel printed multimaterial lattice metamaterials via machine learning and evolutionary algorithm, *Phys. Rev. Appl.* 18 (5) (2022) 054050.
- [51] D. Athinarayanarao, R. Prod'hon, D. Chamoret, H.J. Qi, M. Bodaghi, J.-C. André, F. Demoly, Computational design for 4D printing of topology optimized multi-material active composites, *NPJ. Comput. Mater.* 9 (1) (2023) 1.
- [52] K. Wang, Y.-H. Chang, Y. Chen, C. Zhang, B. Wang, Designable dual-material auxetic metamaterials using three-dimensional printing, *Mater. Des.* 67 (2015) 159–164.
- [53] K.K. Saxena, R. Das, E.P. Calius, 3D printable multimaterial cellular auxetics with tunable stiffness, *arXiv: App. Phys.* (2017).
- [54] Y. Su, X. Wu, J. Shi, A novel 3D printable multimaterial auxetic metamaterial with reinforced structure: improved stiffness and retained auxetic behavior, *Mech. Adv. Mater. Struct.* 29 (3) (2022) 408–418.
- [55] M.J. Mirzaali, M.E. Edens, A.H. de la Nava, S. Janbaz, P. Vena, E.L. Doubrovski, A. A. Zadpoor, Length-scale dependency of biomimetic hard-soft composites, *Sci. Rep.* 8 (1) (2018) 12052.
- [56] M.C. Saldívar, E. Tay, A. Isaakidou, V. Moosabeiki, L.E. Fratila-Apachitei, E. L. Doubrovski, M.J. Mirzaali, A.A. Zadpoor, Bioinspired rational design of bi-material 3D printed soft-hard interfaces, *Nat. Commun.* 14 (1) (2023) 7919.
- [57] M.J. Mirzaali, A. Herranz de la Nava, D. Gunashekar, M. Nouri-Goushki, R.P. E. Veeger, Q. Grossman, L. Angeloni, M.K. Ghatkesar, L.E. Fratila-Apachitei, D. Ruffoni, E.L. Doubrovski, A.A. Zadpoor, Mechanics of bioinspired functionally graded soft-hard composites made by multi-material 3D printing, *Compos. Struct.* 237 (2020) 111867.
- [58] M.C. Saldívar, S. Salehi, R.P. Elias Veeger, E. Tay, M. Fenu, A. Cantamessa, M. Klimopoulou, G. Talò, M. Moretti, S. Lopa, D. Ruffoni, G.J.V.M. van Osch, L. E. Fratila-Apachitei, Z. Doubrovski, M.J. Mirzaali, A.A. Zadpoor, Rational positioning of 3D-printed voxels to realize high-fidelity multifunctional soft-hard interfaces, *Cell Rep. Phys. Sci.* 4 (9) (2023) 101552.
- [59] S. Tabacu, R.F. Negrea, D. Negrea, Experimental, numerical and analytical investigation of 2D tetra-anti-chiral structure under compressive loads, *Thin-Walled Struct.* 155 (2020) 106929.
- [60] F. Albertini, J. Dirrenberger, A. Molotnikov, C. Sollogoub, Computational investigation of the effective mechanical behavior for 3D pre-buckled auxetic lattices, *J. Appl. Mech.* 86 (11) (2019).
- [61] A.G. Mark, S. Palagi, T. Qiu, P. Fischer, Auxetic metamaterial simplifies soft robot design, in: 2016 IEEE International Conference on Robotics and Automation (ICRA), 2016, pp. 4951–4956.
- [62] A. Pal, V. Restrepo, D. Goswami, R.V. Martinez, Exploiting mechanical instabilities in soft robotics: control, sensing, and actuation, *Adv. Mater.* 33 (19) (2021) 2006939.
- [63] F. Vanneste, O. Goury, J. Martínez, S. Lefebvre, H. Delingette, C. Duriez, Anisotropic soft robots based on 3D printed meso-structured materials: design, modeling by homogenization and simulation, *IEEE Robot. Autom. Lett.* 5 (2) (2020) 2380–2386.
- [64] C. Balletti, M. Ballarin, F. Guerra, 3D printing: state of the art and future perspectives, *J. Cult. Herit.* 26 (2017) 172–182.
- [65] M. Chapiro, Current achievements and future outlook for composites in 3D printing, *Reinf. Plast.* 60 (6) (2016) 372–375.